1

OVERVIEW OF DIGITAL RECORDING SYSTEMS

Data storage and retrieval systems are structured under engineering architectural rules. Hard disk drives place data in records that are easily addressed according to known locations at fixed radii and angular positions within a multitude of disk surfaces. Roughly one-third of the cost of a typical disk drive is found in the head and disk components, so an important motive is discovered for increasing the storage density (megabytes per disk) without increasing the number of components. In 1983, a 10-Mbyte 5.25-in. drive (four-disk) price was roughly $500, or $50 per megabyte. In 1987 storage capacity increased to about 400 Mbytes (eight disks) at a price of $2000, or $5 per megabyte. Today (late 1999) 12 Gbytes (12,000 Mbytes) on 3.5-in. drives (two disks) sell at less than $120, or roughly $0.01 per megabyte. Within this time frame, areal density, [bits per inch times tracks per inch (bpi · tpi)] has gone from a few megabits per square inch to about 5 Gbits/in^2, the bit cell has shrunk from roughly 3×70 μm^2 to about 0.09×1.4 μm^2, and data-sensing technology has switched from inductive to magnetoresistive (MR) heads. Over 140 million disk drives were produced in 1998 and virtually all of these drives exploited MR recording heads and longitudinal thin-film media. Manufacturers of recording heads have focused research-and-development (R&D) activities on MR technology, and factories have retooled to supply the industry with MR read heads combined with inductive write heads. Trend-FOCUS (1998) placed the total MR market at 441.5 million units in 1997, which was split 43.2% OEM (original equipment manufacturer) and 56.8% captive disk drive and head manufacturers and claimed that shipments of MR and giant magnetoresistance (GMR) heads totaled 636 and 50.7 million, respectively, in 1998. For 1999 Trend-FOCUS has followed the transition from anisotropic magnetoresistance (AMR) to GMR technology and projects markets of 82.1 and 752.9 million AMR and GMR heads, respectively.

This chapter examines magnetic storage system design requirements for acceptable data integrity at the output of a pulse detector, down through a preamplifier/write driver, and finally to the head and disk components. There are additional levels of error detection and correction hardware and firmware in disk drives that further improve data integrity, but these considerations go beyond the scope of this book. The discussion emphasizes signal, noise, linear and nonlinear effects, and the dependence of a raw (uncorrected) bit error rate (BER) on these factors. Because the writing process creates what is read by the MR sensor, we first briefly discuss the writing of transitions, magnetic properties of recording media, and several transition nonlinearities. As the bit cell shrinks, the requirement for an acceptable BER establishes strong motives for improving the signal amplitude levels and reducing sources of noise and interferences or distortions that degrade the BER to unacceptable levels.

BIT ERROR RATE OF DIGITAL RECORDING SYSTEMS

The BER in high-density disk recording is a subject of intense investigation, and identifying the various sources of error is a significant challenge. Yeh and Wachenschwanz (1997) have studied this problem in systems using sampling detectors known as PRML (partial-response maximum-likelihood) detection; they expanded the concept of signal-to-noise ratio (SNR) to include signal variations arising from linear and nonlinear intersymbol interference (ISI) in pseudorandom sequence (PRS) recording. With Gaussian noise added to random data sequences, the variance in readback amplitude becomes the sum of the noise variance (power) and the ISI variance; they call this the *mean-square error* (MSE) variance. That is,

$$\sigma^2_{\text{MSE}} = \sigma^2_{\text{Noise}} + \sigma^2_{\text{ISI}}, \tag{1.1}$$

so with proper treatment, interference is "noise like" [see Williams, p. 253, in Arnoldussen and Nunnelley (1992)]. Yeh and Wachenschwanz (1997) discuss estimation of the BER using a complementary error function of the signal-to-MSE ratio, where the "signal" is normalized to unity. The relation given in their paper is

$$\text{BER} \sim 0.75 \operatorname{erfc}\left(\frac{1}{2\sqrt{2}\sigma_{\text{MSE}}}\right), \tag{1.2}$$

which is useful as an introduction to the analysis of root causes of bit errors. The analysis of amplitude variations in Viterbi detectors gives a more accurate estimate of BER; however, this subject goes beyond the scope of this book. Archival digital storage systems require extremely low error rates, so (1.2) is plotted on a loglinear basis in Fig. 1.1 to emphasize a raw BER in a design range of roughly 10^{-6}–10^{-10}. As a hypothetical example, assume a design center of BER(z) = 10^{-8}; then $z = 4.05$ approximately satisfies this requirement and a signal [zero-to-peak (0-p)] of

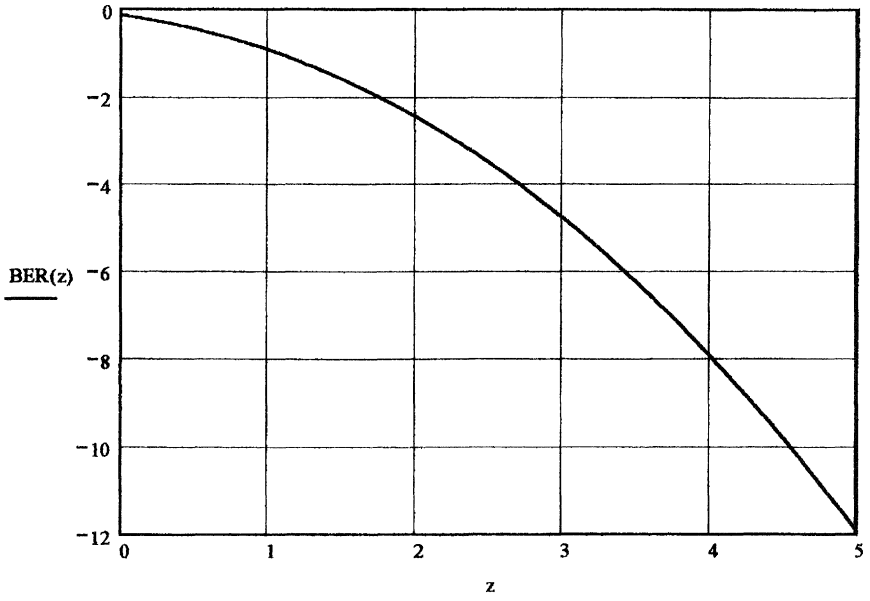

FIGURE 1.1 Log to base 10 of the BER.

$4.05 \times 2.828\sigma_{\text{MSE}}$ would be necessary. To take this idea one step further, assume the system has no ISI variance, or from (1.1), $\sigma_{\text{MSE}} = \sigma_{\text{Noise}}$. Achieving an error rate of 10^{-8} would be roughly equivalent to a signal-to-noise ratio [SNR(0-pk/RMS)] of 11.45, where RMS is the root-mean-square. Expressed in the conventional decibels, $\text{SNR} = 20\log_{10}(11.45) = 21.2$ dB.

At very high bit densities, the nonlinear writing process creates magnetic transitions that are distorted in location and amplitude as a result of magnetic fields from adjacent magnetic transitions. These distortions are sometimes called *nonlinear transition shift* (NLTS) or *nonlinear distortion* (NLD) and *partial erasure* or *nonlinear amplitude loss*. In other words, ISI is composed of linear readback and nonlinear writing phenomena. The reader should consult the literature on magnetic recording signal processing for more on this subject. See, for instance, Yeh and Wachenschwanz (1997), Palmer et al. (1987), or Perkins and Keirn (1995). Extending the example above, if ISI is made equal to noise (perhaps by adding NLTS) the MSE increases on an RMS basis by the factor $2^{1/2}$, or 3 dB, and the BER degrades from 10^{-8} to an unacceptable level of $\text{BER}(4.05/1.414) = 10^{-4.3}$ unless SNR is increased to compensate for the additional NLTS.

SCALING RULES FOR MAGNETIC RECORDING SYSTEMS

Scaling rules of thumb are useful for estimating critical dimensions and relationships in recording systems. There is a correspondence between bit and track densities for

given areal density (AD) points, and for many years disk drive producers have followed bpi/tpi ratios (the *bit cell aspect ratio*) R_{bc} in the approximate range of 15–25, and (AD) is simply given by the relation $AD = R_{bc} \cdot tpi^2 = bpi^2/R_{bc}$. As areal density increases beyond 5 Gbits/in^2, the bit cell aspect ratio appears to be moving to smaller values (R_{bc} values of 8–16 approximately). Justification for this trend arises from the observation that medium noise scales with the square root of track width whereas signal scales directly with width, such that high track densities will be preferred over high bit densities. The rule of thumb for bit cell aspect ratio facilitates exploration of product designs and assessment of consequences regarding track width tolerances for write and read heads and for device specifications. The disk drive industry has followed track width design rules based on the track-to-track distance, or track pitch:

$$\text{Write width} \simeq (0.70-0.9) \cdot \text{track pitch} \tag{1.3}$$

$$\text{Read width} \simeq 0.80 \cdot \text{write width} \simeq (0.60-0.80) \cdot \text{track pitch} \tag{1.4}$$

In recent technology demonstrations at 36 Gbits/in.^{2} the bit cell was 0.044 by 0.41 μm^2 (R_{bc} = 580 kbpi/62 ktpi = 9.3) and the GMR read width was approximately 0.30 μm, or 73% of the track pitch.

SIGNAL AMPLITUDE

Magnetoresistive heads exploit the AMR effect or the GMR effect. In either case, the change in resistance ΔR in a magnetic field divided by the resistance R in the zero-field state defines a figure of merit $\Delta R/R$ that is useful for comparing different technologies and devices. AMR devices commonly have a figure of merit of about 1.5–2%, while GMR/spin valve devices are roughly 4–15%, depending on design and complexity. These devices must be energized with a sense current to produce an electrical signal. That is,

$$\text{Signal} = I\,\Delta R(H) = I\frac{\Delta\rho(H)}{t}\frac{W}{h} \quad \text{(V)} \tag{1.5}$$

where I is the sense current, $\Delta\rho(H)$ is the resistivity change with magnetic field H, t is the film thickness, W is the sensor width, and h is its height. At high areal densities the track width W must reduce; in fact, the geometries and properties of the entire sensor must scale to maintain useful levels of signal. The task of this book is to delve into the details behind (1.5) and examine the design and analysis challenges of MR heads. AMR devices are inherently nonlinear, and one of the many design challenges is to bias the sensor for reasonably linear operation over a useful range of magnetic fields. GMR devices give more signal and have improved linearity but are more complicated and have a number of very thin critical layers in their construction. Because MR devices must be excited with a sense current, they heat up and thermal

issues must be addressed. In addition, MR sense elements require magnetic shielding for operation at high bit densities.

The primary use of shields is to define a limited region of sensitivity to *external* flux for an MR sensor; however, the *internal* magnetic field environment for shielded conductors and magnetic sensors is altered as well. The unshielded sensor of Hunt (1971) produces a pulsewidth that is the geometrical mean of the element height h and its effective spacing $d + a$ from the surface of an arctangent magnetic transition $M_x(x) = (2M_r/\pi)\tan^{-1}(x/a)$,

$$\mathrm{PW50} \simeq \sqrt{4(d+a)(d+a+h)}. \tag{1.6}$$

Mallinson (1996, p. 64) gives an equivalent expression $\mathrm{PW50} = 2[d(d+h)]^{1/2}$ for a sharp transition. It is apparent an unshielded MR sensor would provide unacceptably wide pulses for useful heights $h \sim 1$ μm. Potter (1974) addressed this problem and analyzed a shielded MR sensor as two back-to-back Karlquist heads with the MR element of thickness t centered between shields ($G = g + t + g$). Bertram (1995) modified Potter's expression for the readback flux to include the medium thickness in the effective spacing $y = d + a + \delta/2$. Using a combination of Potter and Bertram, the flux entering a symmetrically shielded MR element for an arctangent transition is

$$\phi(\bar{x}, y) = \frac{2}{\pi} 4\pi M_r\, \delta W \cdot 10^{-8} \frac{y}{g}\left[f\left(\frac{\bar{x}+g+t/2}{y}\right) - f\left(\frac{\bar{x}+t/2}{y}\right) + f\left(\frac{\bar{x}-g-t/2}{y}\right) - f\left(\frac{\bar{x}-t/2}{y}\right)\right], \tag{1.7}$$

where

$$f(z) = z\, \tan^{-1} z - 0.5\, \log_e(1+z^2). \tag{1.8}$$

The flux is in webers for M_r in emu/cm^3 and all dimensions in centimeters (1.0 Maxwell $= 10^{-8}$ Weber.) Normalized plots of (1.7) given by $F(x, y) = \Phi(x, y)/[4\pi M_r\, \delta W \cdot 10^{-8} y/g]$ and a simple Lorentzian function (1.9) are compared in Fig. 1.2. The Lorentzian is defined by the expression

$$L(x) = \frac{V_0}{1 + (2x/\mathrm{PW50})^2}, \tag{1.9}$$

where V_0 is the zero-to-peak signal amplitude, x is the position along a track ($x = vt$, v is the disk surface velocity and t is time). The Lorentzian is physically incorrect as

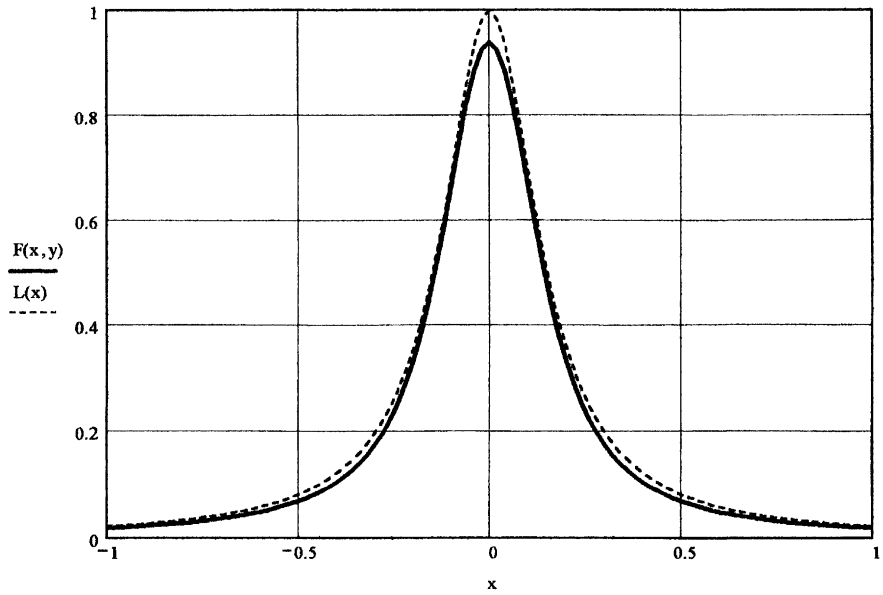

FIGURE 1.2 Comparison of pulses based on $F(x) = x \cdot a\tan(x) - 0.5\ \ln(1 + x^2)$ and the Lorentzian $L(x) = 1/(1 + x^2)$.

a description of the readback process; however, it is simple and its shape approximates that of (1.7). The PW50 is approximated quite well by the relation

$$\text{PW50} \simeq \begin{cases} \left[\dfrac{G_{ss}^2 + t^2}{2} + 4(d + a)(d + a + \delta)\right]^{0.5} & \text{(single element)}, \quad (1.10a) \\ \left[\dfrac{G_{ss}^2 + (g + 2t)^2}{2} + 4(d + a)(d + a + \delta)\right]^{0.5} & \text{(dual element)}, \quad (1.10b) \end{cases}$$

where G_{ss} equals $2g_1 + t$ or $2g_1 + g + 2t$ for single- and dual-element heads, respectively. Other approximations for PW50 are published; for example, see Smith (1991), Champion and Bertram (1995), or Bertram (1995). The parameters d, a, and δ refer to the magnetic spacing (bottom edge of the MR sensor to the magnetic surface of the disk), the length ($L = \pi a$) of the written magnetic transition, and the thickness δ of the magnetic layer on the disk surface, respectively. Each of these parameters will normally be scaled down to produce acceptably narrow pulses for high bit densities. Magnetic spacing d is fundamental to recording physics, and it emerges as a natural basis for scaling the other parameters; systems can be designed using the relations $G_{ss} \simeq 5d$, $a \simeq d$, and $\delta \simeq d/2$, for which PW50 $\simeq 5.7d$. That is, in a well-designed system, PW50 would scale with magnetic spacing. With $G_{ss} = 0.20$ μm, $d + a = 0.10$ μm, $\delta = 0.02$ μm, and stripe height $h = 1.0$ μm,

estimates of shielded and unshielded pulsewidths for a single-element head are approximately 0.26 and 0.66 μm, respectively. That is, shielding can reduce PW50 by more than a factor of 2.

It is common to find that the literature on signal processing treats the readback signal with simple approximations for describing the amplitude and pulse shape. The Lorentzian pulse is especially useful because it agrees with experimental waveforms fairly well, and it has simple analytical properties. When data are stored, sequences of transitions are written, and the readback signal is a linear superposition of the responses to individual transitions. The total response for an infinite sequence of alternating polarity Lorentzians was published by Comstock and Williams (1973):

$$f(x, P, B) = \sum_{n=-\infty}^{\infty} (-1)^n V(x - nB) = V_0 \frac{\pi P}{2B} \frac{\sinh(\pi P/2B)\cos(\pi x/B)}{[\cosh^2(\pi P/2B) - \cos^2(\pi x/B)]} \quad (1.11)$$

where P = PW50 and B is a constant bit cell length or distance between pulses (i.e., $1/B$ = bit density). This result is compact and useful in communicating the essential features of readback signals and amplitude dependence on recording density. Notice the argument scales with P/B, so pulsewidth P must be reduced along with reductions in bit cell length B to maintain useful levels of amplitude. Figure 1.3 shows a family of plots for $f(x, P, B)$ with fixed P and parameter B, while Fig. 1.4 shows the peak signal $f(x = 0, P, B)$ for variable B and parameter P.

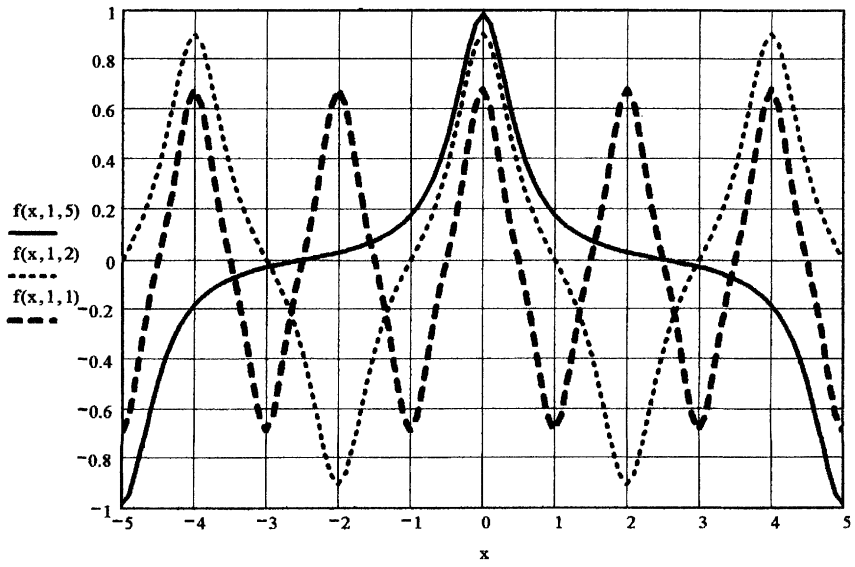

FIGURE 1.3 Normalized signal for infinite sum of alternating polarity Lorentzian pulses given by $f(x, P, B)$, where x is position along a track, P is the pulsewidth (constant at 1.0), and B is the distance between pulses ($B = 1, 2, 5$).

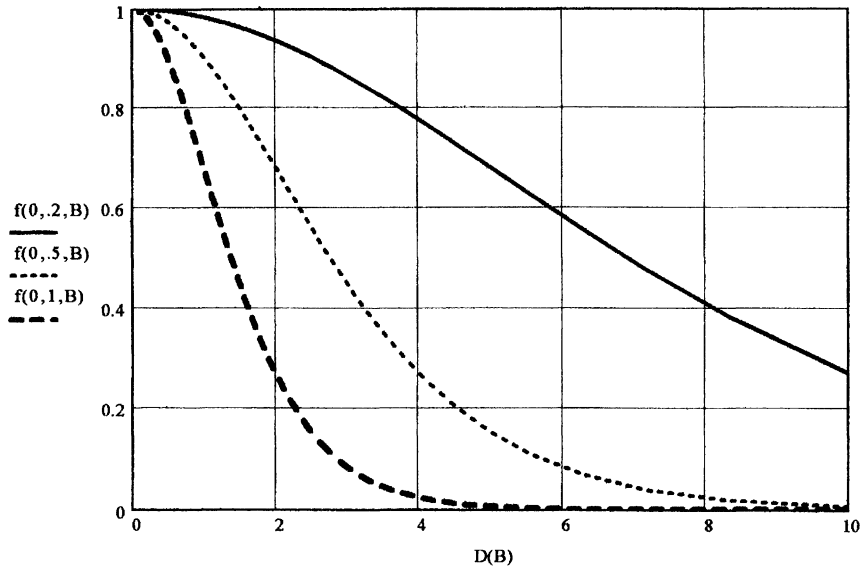

FIGURE 1.4 Normalized zero-to-peak signal for infinite sum of Lorentzians. Pulse peak at $x = 0$ for $P = 0.2$, 0.5, 1.0 units. Linear density $1/B$ is variable.

Signal processing engineers and the designers of detectors have defined the concept of *channel density* as a figure of merit for comparing channels. In the literature, this concept is identified with the relation

$$U = \text{channel density} = \frac{\text{PW50}}{B} = \text{PW50} \cdot \text{linear density}, \tag{1.12}$$

and today's PRML channels operate at useful error rates with U in the range of 2–3 or so. The relation given in (1.11) simplifies further when (1.12) is substituted for P and B:

$$\frac{f(0, P, B)}{V_0} = \frac{(\pi/2)U}{\sinh[(\pi/2)U]} \tag{1.13}$$

Detector channels operating at high user densities (say $U \geq 2.5$) place less burden on head and medium components because PW50 can be somewhat larger for a given linear density ($1/B$), and requirements can be relaxed for G_{ss}, d, a, and δ.

AREAL DENSITY AND MAGNETIC SPACING

The history of rotating disk magnetic storage begins in 1957 with the IBM 350, which was the first production hard disk drive with movable recording heads. The IBM 350 stored data at 2000 bits/in.^{2}, and the magnetic head flew over the disk

surface at a spacing of 800 μin., or 20 μm. Harker et al. (1981) review the first 25 years of disk drive technology and give some details regarding areal densities and critical geometrical parameters of IBM products. By 1981, the IBM 3380 drive was at about 12 Mbits/in.^{2} and heads were flying at 12 μin. (0.30 μm). One of the most critical parameters is the spacing between the recording head gap and the magnetic surface of the medium; this is called the *magnetic spacing*. If the magnetic disk and magnetic head have no protective coatings, then the magnetic spacing nearly equals the flying height of the head. When heads are mechanically lapped and polished, there exists a small recession (70 Å or less) of the head pole tips below the air-bearing surface of the head slider; this is called *pole tip recession* (PTR). Today, all recording heads and disks have a protective overcoat of diamondlike carbon (DLC) or other hard material applied to their surfaces, so the magnetic spacing and flying height are no longer identical.

The relationship of areal density to magnetic spacing is easily derived from PW50, channel density (U), bit cell ratio (R_{bc}), signal amplitude (at the highest density), and the scaling rules developed above. Reading from (1.9), (1.12), and (1.13), the areal density can be written

$$\text{Areal density} = \frac{\text{bpi}^2}{R_{bc}} = \frac{U^2}{R_{bc}\,\text{PW50}^2} = \frac{U^2}{R_{bc}K^2d^2}, \tag{1.14}$$

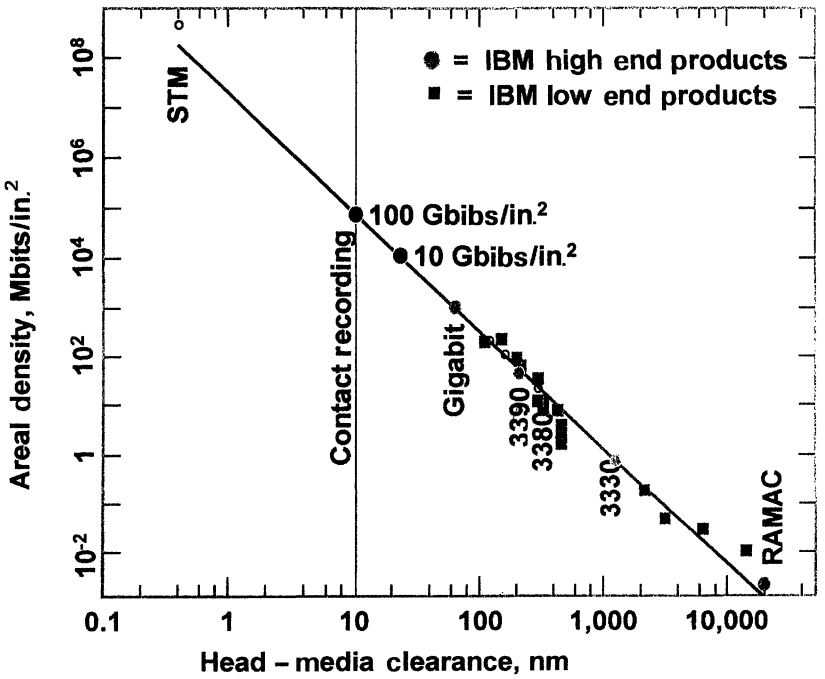

FIGURE 1.5 Areal density as a function of head–medium clearance [from Harker et al. (1981) and Ashar (1997)].

where the scaling rule PW50 = Kd is used. On the log–log plot of Fig. 1.5, (1.14) fits very well the published data of Harker et al. (1981) and Ashar (1997). With overcoats on head sliders and disk surfaces, the actual clearance between head and disk (the "flying height") is nearly $0.50d$. The hard coatings (e.g., DLC) are each normally designed to be roughly $0.25d$, and PTR is held to about $0.10d$. The 3σ tolerance on flying height variations will normally be about 15–20% of the nominal value.

THE WRITTEN TRANSITION

The highly nonlinear writing process can be treated with analytic approximations that give direct and immediate insight regarding the written transition, its magnitude, sharpness, and the dependence of these attributes on the recording head and properties of the magnetic medium. The Williams and Comstock (1971) model has become the archetype for this type of analysis, and their results are given here. They assume a magnetization transition of the form $M(x) = (2M_r/\pi)\tan^{-1}(x/a)$ in a medium whose magnetic properties are described by the remanence M_r, coercivity H_c, coercive squareness S^*, remanent coercivity $H_{\text{cr}} = H_c/r$, $r = (3 + S^*)/4$, and thickness δ. The transition is longitudinal and is written by the x-component of a Karlquist (1954) head,

$$H_x^h(x, y) = \frac{H_0}{\pi}\left[\tan^{-1}\frac{(x + g/2)}{y} - \tan^{-1}\frac{(x - g/2)}{y}\right] \tag{1.15}$$

at a position $H_x^h(x = x_0, y) = H_{\text{cr}}$, where the transition is centered; H_0 is the field at $x = y = 0$ and g is the gap length. The head field gradient is given by

$$\frac{dH_x^h}{dx} = -\frac{QH_c}{y} = \frac{-2x_0H_0}{\pi g H_c}\sin^2\left(\frac{\pi H_c}{H_0}\right)\frac{H_c}{y} \tag{1.16}$$

Here, Q is the normalized write field gradient and is valid only for $H_0 \geq 2H_c$. This relation for Q from Bertram (1994, Chap. 8) is graphed in Fig. 1.6. Williams and Comstock (1971) calculate the intermediate transition (with parameter a_1) that exists at the trailing edge of the energized writing head, and then find the final transition (with parameter a) that exists after the medium has moved far away from the writing head (i.e., the field is turned off) and the transition has relaxed under the influence of its self-demagnetizing field:

$$\frac{a_1}{r} = \frac{y(1 - S^*)}{\pi Q} + \left[\left(\frac{y(1 - S^*)}{\pi Q}\right)^2 + \frac{2M_r\,\delta}{H_c}\frac{2y}{Qr}\right]^{1/2} \tag{1.17}$$

$$a = \frac{a_1}{2r} + \left[\left(\frac{a_1}{2r}\right)^2 + \frac{2\pi M_r\,\delta a_1}{(3 + S^*)H_c}\right]^{1/2} \tag{1.18}$$

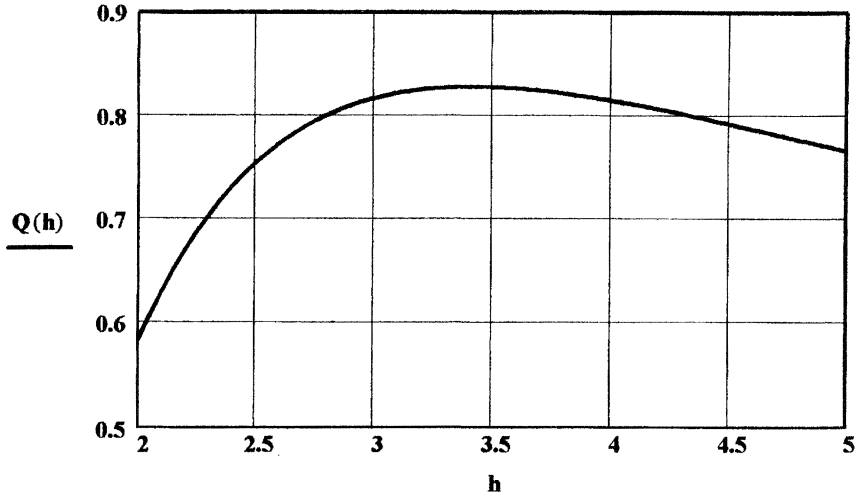

FIGURE 1.6 Normalized head field gradient [Eq. (1.16)] for Karlquist recording head field plotted as a function of normalized field $h = H_0/H_c$, where H_0 is the x-component of the field at $x = 0$, $y = 0$.

The final transition length ($L = \pi a$) is always greater than the intermediate one; that is, the written transition broadens (relaxes) as it moves away from the recording field. Figure 1.7 shows plots of intermediate and final transition parameters; the sharpest transition is obtained at the highest write field gradient. These calculations assume

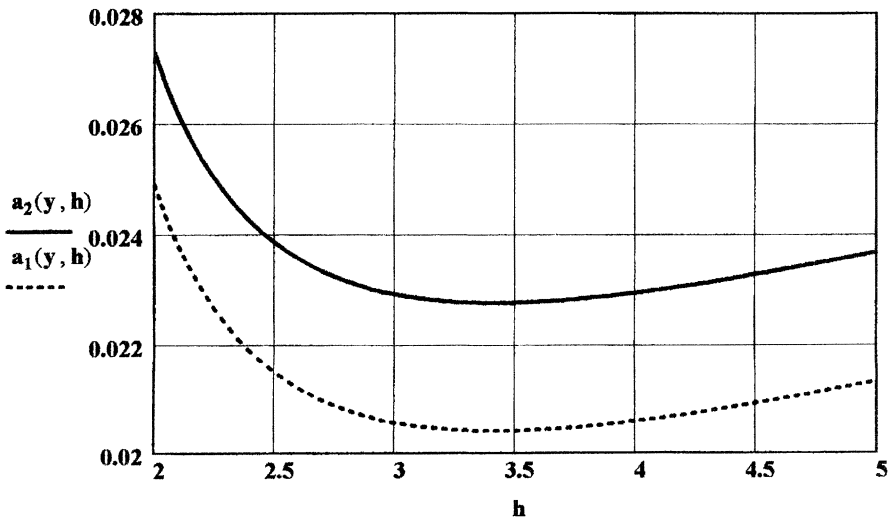

FIGURE 1.7 Williams–Comstock transition parameters for a transition in the presence of the recording field (a_1) and for the relaxed transition (a_2) in the absence of the recording field.

the write head never saturates magnetically, which is almost never the case in practice. When a head goes into saturation, the final transition parameter increases (perhaps by a factor of two- or three-fold in extreme cases) with increasing write current.

MAGNETIC FIELD ABOVE A WRITTEN TRANSITION

The sensing element of an MR head is excited by the magnetic field of written transitions. Potter (1970) analyzed the demagnetizing field for a single arctangent transition written longitudinally in a recording medium. The geometry of the head and medium system is shown in Fig. 1.8. The horizontal (H_x) and vertical (H_y) field components are given by the relations

$$H_x(x,y) = 4M_r\left\{\tan^{-1}\left[\frac{x(\delta/2+y)}{x^2+a^2+|\delta/2+y|a}\right] + \tan^{-1}\left[\frac{x(y-\delta/2)}{x^2+a^2+|\delta/2-y|a}\right]\right\}, \tag{1.19}$$

$$H_y(x,y) = 2M_r \log_e\left[\frac{x^2+(|\delta/2+y|+a)^2}{x^2+(|\delta/2-y|+a)^2}\right]. \tag{1.20}$$

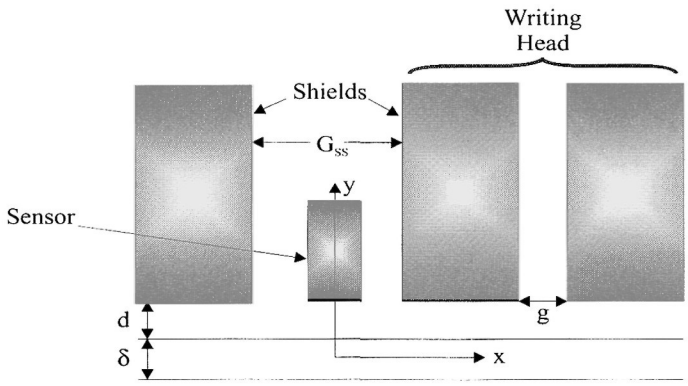

FIGURE 1.8 Geometry of a merged MR read, inductive write head system where the trailing write pole serves as one of the shield layers of the MR device.

The maximum field strength at a distance $y = d + \delta/2$ above the center of the medium is

$$H_y(x = 0, y = d + \delta/2) = 4M_r \log_e\left[\frac{d + a + \delta}{d + a}\right] \simeq \frac{4M_r\,\delta}{d + a} \qquad \text{Oe.} \qquad (1.21)$$

This expression is a useful approximation for estimating the readback signal of an unshielded MR sensor and its dependence on medium properties and head–medium spacing; the injected sensor flux is approximately $\Phi_s \simeq 4\pi W t H_y(x, y)$. The analysis of Potter (1974), leading to the relation given in (1.7), must be used for signal calculations with shielded MR heads.

HEAD AND PREAMPLIFIER NOISE

The major contributions to noise in disk drives are from the magnetic head, the preamplifier, and spatial jitter of written transitions. Head and preamplifier noises arise from electronic thermal fluctuations and obey Gaussian statistics; their noise spectral densities (NSDs) are reasonably constant over the bandwidths of interest and the noise voltage is readily computed using Nyquist's theorem [see Williams, Chap. 7, in Arnoldussen and Nunnelley (1992)]:

$$e_n = \sqrt{4K_B T R(f)\,\Delta f} = \text{NSD}\sqrt{\Delta f} \qquad \text{V, RMS,} \qquad (1.22)$$

where $k_B = 1.3085 \times 10^{-23}$ J/K (Boltzmann's constant), T is the absolute temperature in kelvins, $R(f)$ is the noise-equivalent resistance (in ohms) which depends on frequency (f in hertz), and Δf is the noise bandwidth (in hertz) of the system. Magnetoresistive sensors are designed to meet customer requirements, and today the head designer is normally constrained to a maximum of about 60 Ω noise-equivalent resistance for the MR head (including the electrical connection network); at a temperature of 328 K, the head and connection NSD would be about 1.0 nV/$\sqrt{\text{Hz}}$. Preamplifier NSD varies somewhat, but it is normally in the range of 0.5–0.7 nV/$\sqrt{\text{Hz}}$. The combined electronic NSD from head and preamplifier would then be about 1.2 nV/$\sqrt{\text{Hz}}$, and with a system bandwidth of 100 MHz, the electronic noise voltage would be 12 μV (RMS).

MEDIUM NOISE (JITTER)

Thin-film disk transition jitter is a complicated subject; however, much insight has been developed since about 1983. A recording medium is composed of single-domain magnetic grains roughly 100 Å in diameter with nonmagnetic grain boundaries of 10 Å or less. As magnetic transitions are written along a track, statistical fluctuations in transition position and length arise from the switching

properties of magnetic grains at a particular location; this is called *transition jitter*. Zhu in Chapter 6 of Arnoldussen and Nunnelley (1992) and Bertram (1994) are excellent references to the subject of noise in thin-film media, and many useful papers have appeared in recent years. Tarnopolsky and Pitts (1997) and Xing and Bertram (1997), for example, discuss medium-limited SNR; they show that medium noise power is composed of jitter in transition position and in width. Xing and Bertram show that the normalized noise power spectrum NP(k) for transition noise can be written as

$$\mathrm{NP}(k) = \frac{B}{|V_{\mathrm{iP}}(k)|^2}\mathrm{PSD}(k) \simeq \sigma^2_{\mathrm{jitter}}k^2 + \sigma^2_{\mathrm{width}}k^4, \tag{1.23}$$

where $V_{\mathrm{iP}}(k)$ is the Fourier transform of the isolated pulse and k is the wavenumber. The position and width variances depend on read track width W, transition parameter a and cross-track correlation length s:

$$\sigma^2_{\mathrm{jitter}} = \frac{\pi^4 s a^2}{48W}, \qquad \sigma^2_{\mathrm{width}} = \frac{\pi^4 a^2}{60}\sigma^2_{\mathrm{jitter}}. \tag{1.24}$$

Transition position and width jitter are related to the microstructure, grain size, intergranular coupling, and magnetic properties of the medium. Sato et al. (1996) and McKinlay et al. (1996), for example, discuss these subjects for specific magnetic alloys and relate them to medium noise. Small uniform grain diameters with low intergranular coupling (i.e., nonmagnetic grain boundaries and no exchange coupling between grains) give the best medium-limited SNR because these properties lead to reductions in switching variances at the level of individual grains in the transitions. Scaling rules start breaking down for grain diameters smaller than about 100 Å because thermal fluctuations in the disk magnetization lead to magnetic viscosity or relaxation effects (super-paramagnetism). This deep and broad subject goes beyond the scope of this book; however, a good entry point to a discussion is by Chikazumi and Charap (1978). Examining (1.23) and (1.24) shows if system SNR is limited by medium noise, improvements are bought only by reducing position and width jitter, and these must be scaled down with $B \times \mathrm{PW50}$ without creating reliability problems such as signal decay from thermal relaxation.

It is normal practice to measure medium noise on a spectrum analyzer by subtracting the head and preamplifier noises and integrating the remaining noise over the band of interest; this procedure gives the broad-band noise (voltage or power, depending on equipment setup). Since medium noise is in the transitions, the measured noise increases with linear density. The effective standard deviation of medium noise σ_n (composed of position jitter and "a" jitter) can then be extracted from the data. Typical numbers might be $V_n = \sqrt{P_n}$ (at $B = 100$ nm) $= 20$ μV (RMS), $V_0 = 300$ μV (0-p), and PW50 $= 250$ nm, for which $\sigma_n \simeq 6.9$ nm. Medium jitter is also measured with time-interval analyzers. In this case transitions are normally written at lower densities to facilitate the measurement; however, the jitter values are rather small (say 2–4 nm) compared to jitter at high densities (6–12 nm).

Medium noise is also studied with magnetic force microscopy (MFM), and noisy, high-density recordings show poorly defined transitions with significant percolation of switching clusters between transitions. These micromagnetic problems have been studied extensively by Zhu [see Chap. 6 of Arnoldussen and Nunnelley (1992)].

Xing and Bertram (1997) show that position jitter dominates at low densities and only at very high densities do width fluctuations become significant. In their experiments with thin-film media, the estimates of jitter for hyperbolic tangent and error function transition shapes give nearly the same values. For a disk with $M_r\delta = 0.8$ memu/cm^2 and $H_c = 2200$ Oe, they obtain values for position jitter of 3.7 nm, width jitter of 155 nm^2, cross-track correlation length $s = 18$ nm, and transition parameter $a = 32$ nm with an AMR head width $W = 2.7$ μm.

TOTAL NOISE AND SYSTEM SNR

Head, preamplifier and broad-band integrated medium noises are added to find the total RMS noise:

$$N_t = [N_{\text{head}}^2 + N_{\text{preamp}}^2 + N_{\text{medium}}^2]^{0.5}. \tag{1.25}$$

With our example of head, preamplifier, and medium noises of 10, 7, and 20 μV, respectively, the total RMS noise would be 23.4 μV, and the SNR (for low-density signal V_0 and high-density noise) would be 300/23.4, or 22.1 dB (0-p/RMS). The high-density signal (say, at $U = 2.3$) is estimated with (1.13) and $f(0, P = 2.3B, B) = 0.20V_0$, or 60 μV (0-p).

Partial-response detectors (e.g., PR4 channels) use equalization to shape the incoming pulses in a manner that allows the Viterbi detector to eliminate most of the linear ISI. The signal and noise spectra of PRSs is substantially altered by the equalizer, such that the sampled data seen at the sequence detector differ from the RMS signal and noise. Yeh et al. (1998) show that the SNR of an N-bit PRS sequence is altered according to the relationship

$$\text{SNR}_{\text{sync}}^2 = \frac{2N}{N+1}\text{SNR}_{\text{RMS}}^2 \tag{1.26}$$

and a 31-bit PRS achieves an improvement of $\sqrt{62/32}$, or 2.87 dB, in SNR over the RMS value. Experimentally, they obtained about 25%, or about 2.5 dB, improvement in SNR.

NONLINEAR INTERFERENCES

Partial-response detectors shape the readback pulse to obtain equalized responses that reduce or eliminate much of the linear ISI at the sampling points. Nonlinear interferences or distortions associated with writing at high densities cannot be

equalized out of the data patterns so they increase the MSE and the error rate suffers. These nonlinearities include NLTS, partial erasure, and overwrite. Bertram (1994) analyzes the physics of these issues, and he should be consulted for insight and details; for di-bit patterns NLTS (or displacement Δx) can be written in terms of its ratio to the bit cell length B:

$$\frac{\Delta x}{B} \simeq \frac{4a^2(d + \delta/2)^2}{B^4}. \tag{1.27}$$

Most of the literature on signal processing discusses NLTS or NLD in terms of percentage or decibels relative to the undistorted signal amplitude. Today it is common to find specifications for NLTS at -14 dB (i.e., 20%) or less for uncompensated data. Some compensation may be achieved during the writing process for data patterns having predictable shifting; this is called *write precompensation*, which removes perhaps half of the uncompensated shift, thus yielding about -20 dB (or 10%) NLTS.

Partial erasure arises when transitions are so closely spaced that small regions "percolate" over to adjacent transitions and reverse the magnetization with a concomitant loss of readback flux. The experiments of Lin et al. (1992) show that nonlinear amplitude losses become measurable at bit spacings $B \sim 4a$ and less. Zhu [Chap. 6 in Arnoldussen and Nunnelley (1992)] analyzes the physics of this micromagnetic problem.

In thin-film recording, "overwrite" is primarily the result of shifting "hard" transitions relative to "easy" transitions when writing new data over old data patterns. Hard transitions are those in which the magnetization is written in a direction opposite to the magnetization just entering the writing zone; easy transitions are those where the head field writes the magnetization in the same direction as the magnetization entering the write zone. Thus transition positions are modulated by the polarities of incoming old data, and this creates interesting phase modulation spectra. For special cases of new and old patterns (with imaging not included), Bertram (1994) shows that hard transition shifting Δ can be expressed as

$$\Delta \simeq \frac{M_r\, \delta(d + \delta/2)}{2x_0 \pi Q H_c}, \tag{1.28}$$

where $2x_0$ is the size of the writing zone and Q is defined in (1.16). Under most head and medium conditions, hard transition shifting will be less than a few percent of the high-density bit length B and overwrite will not substantially degrade the BER. Yeh and Wachenschwanz (1997) show -30 dB overwrite gives "less than a factor of 2 increase in BER, which is almost equal to the intrinsic uncertainty in BER measurement."

TOP-DOWN DESIGN OF A RECORDING SYSTEM

This introductory chapter ends with a high-level view of recording system design, starting with a BER requirement and spreading the noise and interference budgets over the system components. This "top-down" approach is discussed by Yeh et al. (1998), and their prescription includes noise and ISI reduction of 25% by sequence (Viterbi) detection. All noises and interferences are expressed as percentages of the sampled signal level (normalized to 1.0) in a partial-response channel, and (1.1) and (1.2) above are used to create the budget. Figure 1.9 is a flow diagram of the results, taking BER(4.32) = 10^{-9} and democratically splitting the noise and nonlinear ISI into equal parts of 5.8% each (after sequence detection.)

The noise budget is split equally between medium and system contributions (again, democracy in magnetic recording), or 5.5% each; that is, the medium SNR would be 25.2 dB (0-p/RMS), and the system noise is spread 4.5% for the head and 3.2% for the preamplifier electronics. In other words, the head SNR should be 26.9 dB (0-pk/RMS) after equalization in a PR4 channel. Figure 1.10 shows projections of the areal density achievable for a given readback sensitivity measured in millivolts [peak-peak (p-p)] per micrometer of sensor width. The curves are based on a low-density signal requirement of 1.00 mV before equalization; the solid curve allows the bit cell ratio (R_{bc}) to vary from 15 : 1 at low areal densities to 4.0 : 1 at high densities, whereas the dotted curve assumes $R_{bc} = 4.0$ at all densities. In Chapter 5, the reader will find analyses of soft adjacent-layer (SAL) biased AMR heads with sensitivites of 0.7–1.36 mV/μm that can support areal densities in the range of 3–6 Gbits/in.^{2} at bit cell ratios of approximately 15 : 1–18 : 1. Chapter 6 is devoted to the design and

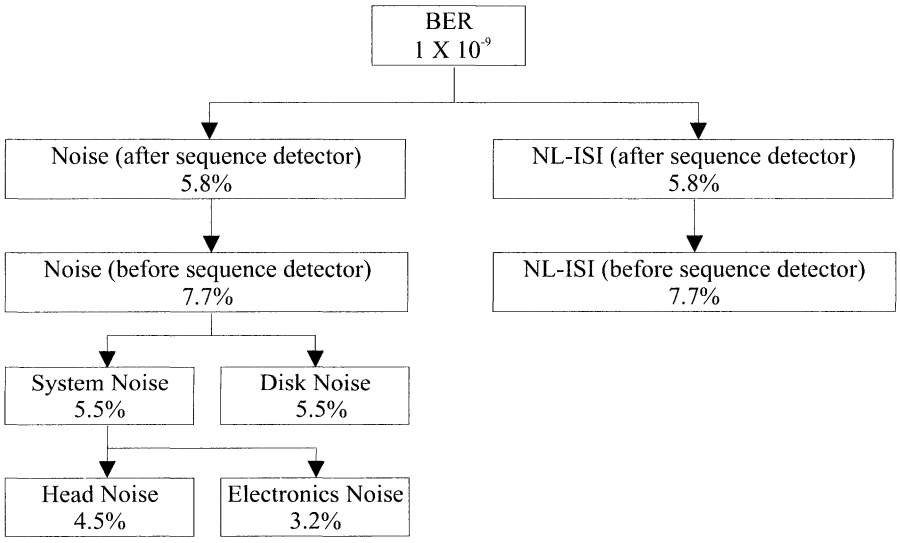

FIGURE 1.9 Top-down approach for a recording system designed to support a BER of 10^{-9} (from Yeh et al., 1998).

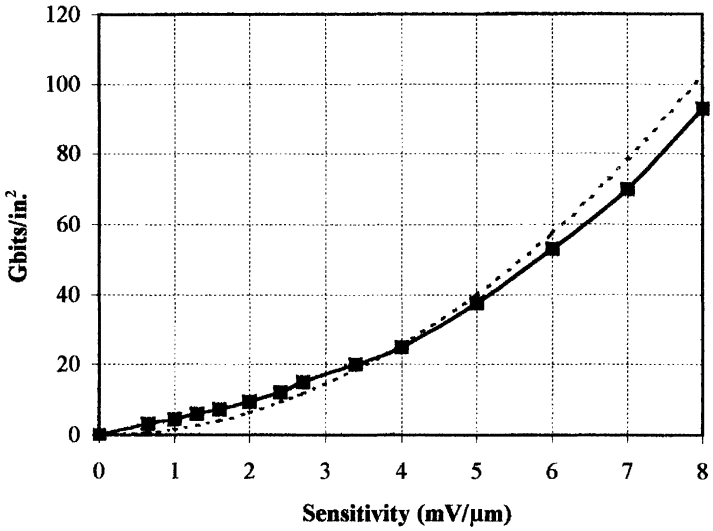

FIGURE 1.10 Areal density projections for read signal sensitivities in millivolts per micrometer of sensor width based on a low-density signal requirement of 1.0 mV (p-p) before equalization. Solid curve: the bit cell ratio R_{bc} varies from 15 : 1 at low areal density to 4 : 1 at high areal density. Dotted curve: $R_{bc} = 4.0$ at all areal densities.

analysis of GMR spin valve sensors with sensitivities at 0.8–5.4 mV/μm; the possibility of improving the sensitivity of dual synthetic spin valves (DSSVs) to about 8 mV/μm opens up the application to areal densities of 90 Gbits/in.^{2} or greater.

REFERENCES

Arnoldussen, T. and Nunnelley, L., Eds., *Noise in Digital Recording*, World Scientific, Singapore, 1992.

Ashar, K. G., *Magnetic Disk Drive Technology*, IEEE Press, New York, 1997.

Bertram, H. N., *Theory of Magnetic Recording*, Cambridge University Press, 1994.

Bertram, H. N., *IEEE Trans. Magn.*, **MAG-31**, 2573 (1995).

Champion, E. and Bertram, H. N., *IEEE Trans. Magn.*, **MAG-31**, 2461 (1995).

Chikazumi, S. and Charap, S., Chap. 15 in *Physics of Magnetism*, Krieger, Malabar, 1978.

Comstock, R. and Williams, M., *IEEE Trans. Magn.*, **MAG-9**, 342 (1973).

Harker, J. M., Brede, D. W., Pattison, R. E., Santana, G. R., and Taft, L. G., *IBM J. Res. Devel.*, **25**, 677 (1981).

Hunt, R. P., *IEEE Trans. Magn.*, **MAG-7**, 150 (1971).

Karlquist, O., *Trans. Roy. Inst. Tech., Stockholm*, **86**, 3 (1954).

Lin, H., Barndt, R., Bertram, N., and Wolf, J., *IEEE Trans. Magn.*, **MAG-28**, 3279 (1992).

Mallinson, J. C., *Magneto-Resistive Heads, Fundamentals and Applications*, Academic Press, San Diego, 1996.

McKinlay, S., Fussing, N., Sinclair, R., and Doerner, M., *IEEE Trans. Magn.*, **MAG-32**, 3587 (1996).

Palmer, D., Ziperovich, P., and Wood, R., *IEEE Trans. Magn.*, **MAG-23**, 2377 (1987).

Perkins, T. and Keirn, Z., *IEEE Trans. Magn.*, **MAG-31**, 1109 (1995).

Potter, R. I., *J. Appl. Phys.*, **41**, 1647 (1970).

Potter, R. I., *IEEE Trans. Magn.*, **MAG-10**, 502 (1974).

Sato, H., Nakai, J., Kikuchi, A., Mitsuya, H., Shimatsu, T., and Takahashi, M., *IEEE Trans. Magn.*, **MAG-32**, 3596 (1996).

Smith, R. L., *IEEE Trans. Magn.*, **MAG-27**, 4561 (1991).

Tarnopolsky, G. and Pitts, P., *J. Appl. Phys.*, **81**(8), 4837 (1997).

Williams, E., Chap. 7 in *Noise in Digital Recording*, Arnoldussen, T. C. and Nunnelley, L. L. (Eds), World Scientific, Singapore, 1992.

Williams, M. and Comstock, R., *Proc. 17th Ann. AIP Conf.*, **5**, 738 (1971).

Xing, X. and Bertram, N., *IEEE Trans. Magn.*, **MAG-33**, 2959 (1997).

Yeh, N. and Wachenschwanz, D., *IEEE Trans. Magn.*, **MAG-33**, 2962 (1997).

Yeh, N., Wachenschwanz, D., and Wei, L., *IEEE Trans. Magn.*, **35**, 776 (1999).

Zhu, J., Chap. 6 in *Noise in Digital Recording*, Arnoldussen, T. C. and Nunnelley, L. L. (Eds.), World Scientific, Singapore, 1992.